JOURNAL OF CHEMICAL INFORMATION AND MODELING

Article

pubs.acs.org/jcim

Modeling the Interface between Islet Amyloid Polypeptide and Insulin-Based Aggregation Inhibitors: Correlation to Aggregation Kinetics and Membrane Damage

Hector Figueroa, Durgaprasad Peddi, Joshua M. Osborne, Brenan M. Wilson, Ranadheer Reddy Pesaru, Balakrishna Kurva, Swathi Ramaraju, Maria C. Milletti, and Deborah L. Heyl*

Chemistry Department, Eastern Michigan University, Ypsilanti, Michigan 48197, United States

Supporting Information

ABSTRACT: Human islet amyloid polypeptide (hIAPP) forms cytotoxic fibrils in type-2 diabetes and insulin is known to inhibit formation of these aggregates. In this study, a series of insulin-based inhibitors were synthesized and assessed for their ability to slow aggregation and impact hIAPP-induced membrane damage. Computational studies were employed to examine the underlying mechanism of inhibition. Overall, all compounds were able to slow aggregation at sufficiently high concentrations (10× molar excess); however, only two peptides showed any inhibitory capability at the 1:1 molar ratio (EALYLV and VEALYLV). The results of density functional calculations suggest this is due to the strength of a salt bridge formed with the Arg11 side chain of hIAPP and the inhibitors' ability to span from the Arg11 to past the Phe15 residue of hIAPP, blocking one of the principal amyloidogenic regions of the molecule. Unexpectedly, slowing fibrillogenesis actually increased damage to lipid membranes, suggesting that the aggregation process itself, rather than the fibrilized peptide, may be the cause of cytotoxicity in vivo.

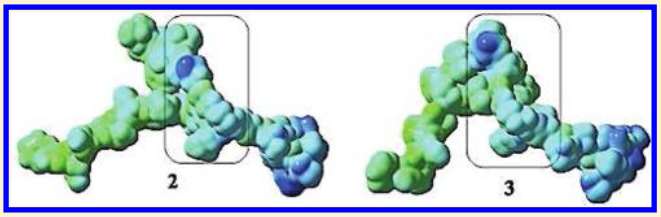

INTRODUCTION

In type-2 diabetes, amyloid plaques slowly replace the insulin-secreting β-cells of the pancreas. The primary component of these plaques is human islet amyloid polypeptide (hIAPP, or amylin), a 37-residue polypeptide that is normally stored alongside and secreted with insulin, and which functions in maintaining glucose homeostasis in the body.[1] Interestingly, hIAPP rapidly forms numerous, dense fibrils in vitro at concentrations as low as 5 μM;[1−3] however, in vivo the peptide remains soluble, despite being stored in secretory vesicles with local concentrations near 800 μM.[3,4] It has been found that insulin itself is a potent inhibitor of hIAPP aggregation[1,2,5] and it is likely that interactions between these two molecules in the secretory vesicles of pancreatic cells are responsible for the absence of amyloid plaques in healthy individuals. Consequently, we have begun to investigate the use of short, insulin-derived peptides as inhibitors of hIAPP aggregation and, therefore, as a potential treatment for type-2 diabetes.

Along the length of hIAPP there exist three discrete, but somewhat overlapping segments capable of forming fibrils: regions 8−20, 20−29, and 30−37.[6−10] These regions have each shown the ability to form aggregates as distinct units separated from the rest of the hIAPP molecule. Aggregation appears to occur in a nucleation-dependent manner,[2,3] and it is believed that hIAPP transitions from soluble randomly coiled monomers to highly ordered aggregates consisting mainly of β-sheet structures.[11,12] This transition may be mediated by an α-helical intermediate.[11]

Despite the numerous amyloidogenic regions, insulin has been shown to bind primarily to the 7−19 region of hIAPP, via the 10−19 region of its B-chain.[5,13] Binding of insulin is believed to maintain hIAPP in a random-coil suite of conformations,[12] which may prevent it from forming the β-sheet structures necessary for aggregation. However, some research has shown that insulin is also capable of binding preformed IAPP aggregates and may actually work by preventing the elongation of already existing fibers.[2] It seems likely that insulin contains multiple binding sites for hIAPP since even substoichiometric amounts of insulin alter aggregation kinetics significantly.[2]

An NMR study of rat IAPP complexed with insulin showed a transiently populated helical structure in residues 11−18 of rIAPP that was important for interaction with insulin.[14] Both hydrophobic and electrostatic forces mediated the intermolecular interactions, specifically positively charged residues of IAPP near the N-terminus with Glu13 of the insulin B-chain. Chemical shifts indicated a binding interface that included Glu13 to Leu17 (EALYL) as well as some surrounding residues. Hydrophobic contacts were surmised to be important, notably Ala14 and Leu17 of insulin and LANFLV of IAPP, within the interface. Subsequent modeling supported an

Received: March 5, 2012
Published: May 3, 2012

dx.doi.org/10.1021/ci300119c | J. Chem. Inf. Model. 2012, 52, 1298−1307

electrostatic interaction between Glu13 of insulin and Arg11 of rIAPP; results were extrapolated to suggest similar probable interactions between the insulin B-chain and hIAPP due to sequence homology in that region.[14] The sequence variation from Arg18 in rIAPP to the less protonated His18 in hIAPP lessens the probability of ionic interaction here in the human form, but Arg11 of hIAPP also is capable of forming the salt bridge with insulin's Glu13.[14] The binding of insulin to the same region of IAPP that interacts with the cell membrane and facilitates self-assembly may sequester this region and reduce fibril formation.

The cytotoxic effects of hIAPP are poorly understood. Mature fibers formed from hIAPP in solution are only minimally cytotoxic to β-cells, implying that the pathogenic effects of the amyloid deposits result from the mechanism of fibril formation and not simply the presence of amyloid fibrils.[15] While these effects are believed to be the result of membrane damage, whether membranes are compromised by the formation of pores or by complete disruption is debated. Synthetic hIAPP in planar lipid bilayers was shown in vitro to form pore structures with five subunits, suggested to represent hIAPP monomers.[16] These pores exhibited ion-permeable channel like activity in the bilayers indicating that the pores may become incorporated within membranes in vivo, changing membrane permeability.[16] The aggregation of hIAPP also distorts membrane structure with the linear growth of amyloid fibers, which are rigidly attached to the flexible cell membrane resulting in membrane curvature.[17] This may lead to greater permeability to small solutes and even membrane fragmentation.[17]

In this study, we have designed and synthesized a series of potential inhibitors, using different length segments of the 10−18 region of the insulin B-chain (the fragment of insulin that reportedly makes direct contact with hIAPP; HLVEALYLV). The sequence of each inhibitor is shown in Figure 1, along with

Figure 1. Sequence of human islet amyloid polypeptide (hIAPP) with amyloidogenic regions highlighted. The sequence of each inhibitor synthesized is also given, with the position meant to indicate generally how the two molecules were aligned for the computational studies (see the Details of the Calculations section for more information). The Arg11 and glutamate residues believed to be crucial for inhibitor binding are underlined.

the sequence of hIAPP; regions important for fibril formation are highlighted. Using model liposomes, these inhibitors were assessed for their ability to slow hIAPP aggregation and decrease membrane damage. Additionally, computational studies were employed to investigate the underlying mechanism of inhibition.

MATERIALS AND METHODS

Peptide Synthesis. Full length human amylin was purchased from SynBioSci (Livermore, CA). Samples were dissolved in hexafluoroisopropanol (HFIP), aliquoted, frozen, and lyophilized. All regular protected amino acids were purchased from Bachem Americas, Inc. (Torrance, CA), Anaspec (Freemont, CA), and Synthetech, Inc. (Albany, OR). Coupling agents and resins were purchased from Bachem Americas, Inc. and Midwest Biotech, Inc. (Fishers, IN). Solvents and deprotecting agents were obtained from Fisher Scientific (Pittsburgh, PA) and Sigma-Aldrich Chemical Co. (St. Louis, MO). The peptides were prepared on a PS3 Automated Peptide Synthesizer from Protein Technologies (Tucson, AZ) using standard solid phase techniques for *N*-α-fluorenylmethyloxycarbonyl (Fmoc) protected amino acids on Rink amide *p*-methylbenzhydrylamine (MBHA) resin (0.64 mmol/g) on a 0.1 mmol scale. This resin produces a C-terminal carboxamide upon cleavage. The side chains of Tyr and Glu were protected as the *t*-butyl derivatives, and His as the trityl form. The deprotection solution for the *N*-terminal amine was 20% piperidine in *N*,*N*-dimethylformamide (DMF). *O*-(Benzotriazol-1yl)-1,1,3,3-tetramethyluronium hexafluorophosphate (HBTU) was used as a coupling agent, activated by 0.4 M *N*,*N*-diisopropylethylamine (DIEA) in DMF. Simultaneous deprotection and cleavage from the resin were accomplished by treatment with 11 mL 90% trifluororacetic acid (TFA)/10% scavenger cocktail (anisole, thioanisole, phenol, water), as previously described.[18] Crude peptides were purified to homogeneity by preparative reversed-phase high performance liquid chromatography (RP-HPLC) on a Waters (Milford, MA) instrument with a Phenomenex (Torrance, CA) Jupiter C18 column (2.2 × 25.0 cm, 10 mL/min). A linear gradient of 10% acetonitrile (0.1% TFA)/water (0.1% TFA) to 50% acetonitrile (0.1% TFA)/water (0.1% TFA) was employed, followed by lyophilization.

Peptide Analysis. Peptide purity was assessed by analytical RP-HPLC. Peaks were monitored at 214, 230, 254, and 280 nm. All synthesized peptides were ≥97% pure as analyzed by peak integration. Electrospray mass spectrometry confirmed the appropriate molecular weights (see Supporting Information Table S1 online).

Preparation of Large Unilamellar Vesicles (LUVs) and Dye Leakage Assay. Lipids were purchased from Avanti Polar Lipids (Alabaster, AL), and carboxyfluorescein was purchased from Sigma-Aldrich (St. Louis, MO). Lipid vesicles were created to encapsulate carboxyfluorescein, which upon disruption of the membrane leaks into the surrounding buffer. Its concentration then gives an indication as to the degree to which the membrane is permeabilized by the peptide. Baseline controls were compared to runs with added peptide and added detergent (which acted as a positive control to give 100% leakage).

The protocols for LUV preparation and the dye leakage assay have been described previously.[18] Briefly, vesicles were prepared by taking 5 mg of a 7:3 ratio of the lipids 1,2-dioleoyl-*sn*-glycero-3-phosphocholine (DOPC) and 1,2-dioleoyl-*sn*-glycero-3-(phospho-L-serine) (DOPS), respectively, and dissolving it in 2 mL of chloroform. The chloroform was evaporated by a gaseous nitrogen stream to create a thin film of lipid on the side of a test tube, which was then dried in a vacuum desiccator overnight. A 500 μL portion of 30 mM carboxyfluorescein dye in pH 7.5 sodium phosphate buffer solution was added to the dried lipid to make multilamellar vesicles (MLVs). This solution was vortexed thoroughly to mix the components and then subsequently frozen using liquid nitrogen and thawed five times consecutively. The solution was then extruded 21 times through polycarbonate filters (pore size 100 nm) using a mini-extruder from Avanti Polar Lipids, fitted with two 0.5 mL Hamilton gastight syringes, producing large unilamellar vesicles (LUVs). To remove nonencapsulated

carboxyfluorescein, the LUV solution was placed on a Sephadex G50 gel exclusion column and the first colored fragment, the separated dye-containing vesicles, was collected. A vesicle solution without dye was made the same way except that it lacked carboxyfluorescein and was not run through the gel exclusion column. For the assay, a sample of the dyed vesicle solution was diluted 10-fold with the vesicle solution without dye so that the stock vesicle concentration was 15.5 ± 1.5 mM.

In this study, to make the peptide solutions, a weighed sample of the purified peptide (hIAPP or inhibitor) was dissolved in a measured volume of dimethyl sulfoxide (DMSO) and vortexed for one minute. Previous control runs in the absence of peptide confirmed that DMSO itself did not induce dye leakage. In addition, control runs on insulin-based fragments confirmed minimal effects to the LUVs by the inhibitor peptides alone, even at the maximal concentration tested. An aliquot of 40 μL of the vesicle solution was added to sodium phosphate buffer to a final volume of 3 mL in a 5 mL test tube. The peptide solutions were added in aliquots, in increasing amounts of inhibitor per sample while the hIAPP concentration was kept constant at 10 μM; the concentrations of inhibitor peptides varied from 0 to 100 μM, so that runs in the absence of inhibitor could be compared to those in the presence of inhibitor peptides at specified ratios to hIAPP. Upon adding the peptide solutions, the test tubes were mixed by inversion, and 300 μL from each tube was transferred to a well in a 96-well plate, which was inserted into the FLx 800 Fluorescence Microplate Reader (BioTek Instruments, Winooski, VT) with KC4 software (filter set to 485 nm excitation, 528 nm emission). A time-course fluorescence spectrum was taken over 180 min. The control used to determine 100% leakage was detergent, 40 μL Triton X (10% v/v in buffer), which induced the release of any remaining dye from vesicles, resulting in the highest possible fluorescence. Dye leakage was reported by the equation:

$$\text{percentage of dye leakage} = (F - F_{\text{baseline}})/(F_{\text{detergent}} - F_{\text{baseline}})$$

where F_{baseline} was the fluorescence of the LUVs in the absence of peptide (solvent only). The spectra were saved and compiled in Microsoft Excel. Since little time dependence was observed, the percentage of dye leakage was averaged over the three hour time period. All assays were run in triplicate and average values are reported.

Thioflavin T (ThT) Assay. Thioflavin T was purchased from Sigma-Aldrich (St. Louis, MO). The ThT assay has been described previously.[15,18] Briefly, vesicles of 7:3 DOPC/DOPS were prepared as described above. The conditions for the ThT experiments were the same as for the leakage experiments, except that tubes contained 25 μM ThT, and carboxyfluorescein was absent; hIAPP concentration was held constant at 10 μM while inhibitor peptide concentration ranged from 0–100 μM. The 96-well plate was placed in the FLx 800 Fluorescence Microplate Reader with KC4 software (filter set to 450 nm excitation, 485 nm emission). A time-course fluorescence spectrum was taken over 300 min. Each assay was run in triplicate. A sigmoidal increase in fluorescence intensity over time indicated fiber formation. The $t_{1/2}$ of each run was calculated from the plot for comparison.

Details of the Calculations. The Gaussian 09 package[19] was used for all calculations and GaussView[20] was employed to create and modify the hIAPP molecule and potential inhibitors. Geometry optimizations were performed using density functional theory (DFT)[21−24] via the Becke three parameter hybrid functional[25] with the Lee−Yang−Parr correlation functional[26−28] and the 3-21G* basis set.[29−34] An electron population analysis was carried out using the Natural Bond Orbital (NBO) framework[35−42] on each optimized inhibitor/hIAPP complex.

Truncated versions of both insulin and hIAPP have been used by others to find the regions of each peptide which associate with one another, and the amyloidogenic regions of hIAPP.[5−10] Therefore, we decided to use a truncated version of hIAPP in this work in an attempt to lower the computational costs. Specifically, hIAPP was cut at the Phe23 residue and a carboxamide terminus was applied. This site was chosen because it did not interfere with the region of hIAPP that binds insulin. Additionally, hIAPP contains a His18 residue, which in vivo exists in two protonation states (pK_a = 6.04). Because our model liposome experiments were carried out at pH 7.5, in order to mimic the extracellular environment in which hIAPP is thought to aggregate and damage membranes, the unprotonated form of His18 was used in the modeling studies, as this is the predominant form at pH 7.5 (~97%).

The inhibitors studied here represent increasingly longer stretches of the 10−18 region of the insulin B-chain, which is known to bind hIAPP. Crystal structures of hIAPP fused to maltose-binding protein[13] suggest that the Phe15 residue of IAPP may stack with the Tyr16 from insulin and that the Arg11 side chain of IAPP is in proximity to insulin's Glu13 residue. In accord with this, each inhibitor was initially aligned by placing the two aforementioned aromatic rings "atop" one another (π-stacking) at a distance of approximately 3 Å, and then placing the glutamate side chain within hydrogen-bonding distance of the Arg11 side chain (no more than 2.0 Å apart). For inhibitor-1, which lacks a glutamate residue, the aromatic rings were aligned and the inhibitor was positioned in an analogous manner.

Inhibitor-5 contains an *N*-terminal histidine residue, which provides another side chain able to participate in hydrogen bonding. Therefore the initial alignment included the usual Arg-Glu salt bridge and, in addition, the His1 side chain was placed in proximity to the Thr9 side chain of hIAPP (~2 Å apart). This was predicted to be a favorable interaction, somewhat analogous to the catalytic triad of serine proteases (Asp-His-Ser). Carboxamide termini were used for all inhibitors to decrease reactivity and for consistency with synthesized peptides.

RESULTS

Because insulin is a known inhibitor of hIAPP aggregation,[1,2,5] we used insulin as a control to compare the relative efficacy of each inhibitor. Our model liposomes are composed of a 7:3 mixture of DOPC:DOPS (see Materials and Methods). In these systems, consistent with other laboratories using different methods,[1,2,5] insulin was found to significantly slow the rate of hIAPP aggregation, even at substoichiometric concentrations. Table 1 compares the $t_{1/2}$ of conversion to fibers for 10 μM hIAPP in the presence of varied amounts of insulin. Conversion times increased from 28 min without insulin to approximately 4 h when 100 μM insulin was added.

Figure 2 below summarizes the results of the dye leakage assay, which was used to measure the extent of hIAPP-induced membrane damage in the presence of 10 μM hIAPP and varied amounts of inhibitor (or insulin). In all cases, the percent leakage of fluorescent dye from vesicles was calculated in

Table 1. Impact of Insulin on hIAPP Aggregation Kinetics

insulin concentration (10 μM hIAPP)	$t_{1/2}$ of conversion to fibers
0 μM	28 min
2 μM	49 min
10 μM	90 min
50 μM	129 min
100 μM	239 min

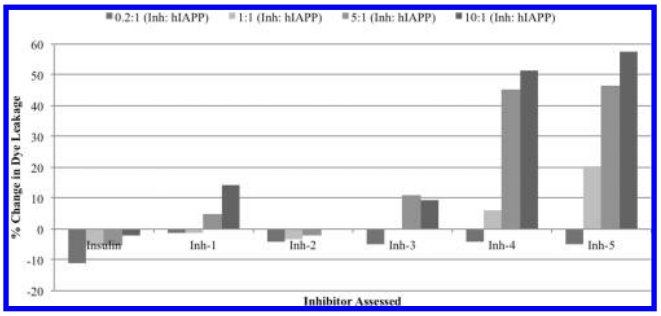

Figure 2. Summarized results of dye leakage assay, used to determine the extent of membrane damage. Bars extending upward indicate greater leakage, while those going down show a reduction in dye leakage. All model liposomes contained 10 μM hIAPP, with varied amounts of inhibitor (or insulin). Data points represent the average of three trials, and the values have been converted to relative change compared to a control vesicle sample containing only hIAPP run concurrently. Error varied with each trial, but remained within 5−10% for all readings. Counterintuitively, higher concentrations of inhibitor led in all cases to greater relative membrane damage. In fact, only inhibitor-2 and insulin showed a reduction in membrane damage at all concentrations. The increase in dye leakage is proportional to the concentration of inhibitor used (see Supporting Information Figure S1).

triplicate, and average values were obtained. Data points were converted to relative changes as compared to hIAPP-treated vesicles without an inhibitor (i.e., without insulin or synthesized peptide) run concurrent with experimental samples. In the figure, bars extending in the positive y-direction therefore indicate greater membrane damage while those in the negative y-direction show a decrease in the extent of membrane damage.

Counterintuitively, higher concentrations of inhibitor actually led to increased membrane damage. This pattern was also seen with insulin, which showed a relative rise in membrane damage as the concentration increased. Other than insulin, only inhibitor-2 (sequence EALYLV) showed a reduction in membrane damage at all concentrations tested, and this reduction was minimal (less than 5%). Inhibitors-1, -3, -4, and -5 increased the release of dye from the vesicles at concentrations at or above 10 μM (equimolar to hIAPP). In fact, the increase in dye leakage seems to be proportional to the concentration of inhibitor used (see Supporting Information Figure S1; R^2 values range from 0.744 for inhibitor-1 to 0.999 for inhibitor-5).

The effects of each inhibitor on hIAPP aggregation were determined using a Thioflavin T fluorescence assay with model liposomes containing 10 μM hIAPP and varied concentrations of inhibitor (or insulin). Trials were run in triplicate and the average value of the $t_{1/2}$ of conversion to fibers was obtained. As with the dye leakage assay, data points were converted to relative changes as compared to hIAPP-treated vesicles without inhibitor or insulin. The results of this assay are summarized in Figure 3, in which bars extending in the positive y-direction

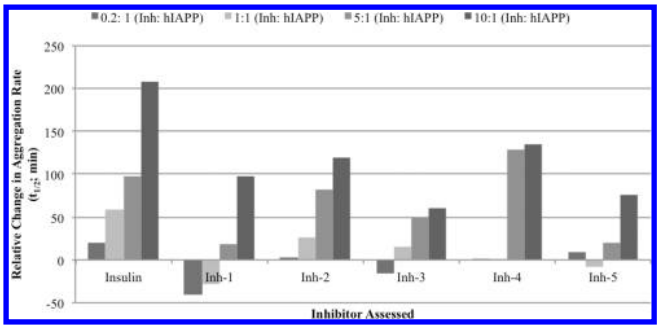

Figure 3. Summarized results of the Thioflavin T fluorescence assay, showing the relative change in the rate of hIAPP aggregation (10 μM) in the presence of varied concentrations of inhibitor (or insulin). Bars above the x-axis represent slower rates of aggregation, while bars below the x-axis indicate an acceleration of aggregation. Results represent an average from three runs and have been converted to relative changes as compared to a vesicle sample containing only hIAPP run concurrently. Error varied with each trial but remained within 5−10% for all readings. All inhibitors were able to slow aggregation at high molar ratios; however, only inhibitors-2 and -3 showed any efficacy at the 1:1 molar ratio. This may be due to their ability to "bridge" hIAPP along one of its principal amyloidogenic regions (see Figure 4). Note that no inhibitor matches the efficacy of insulin.

indicate slower aggregation and bars extending in the negative y-direction show accelerated aggregation. While all inhibitors were able to slow aggregation at high molar ratios (10:1 inhibitor:hIAPP), only inhibitors-2 and -3 showed any efficacy at the 1:1 ratio (EALYLV and VEALYLV, respectively), and some actually accelerated the aggregation process. There does not appear to be any correlation between inhibitor length and change in aggregation kinetics; however, the change in rate of aggregation for each inhibitor, as well as for insulin, is linearly proportional to the concentration of inhibitor used (see Supporting Information Figure S2; R^2 values range from 0.811 for inhibitor-4 to 0.996 for inhibitor-1), suggesting that each compound is interacting with hIAPP in a similar manner to its corresponding region in the full length B-chain of insulin.

In an attempt to rationalize the data obtained about each inhibitor's ability to change the rate of aggregation, computational studies were performed to characterize the interface between each inhibitor and hIAPP. Density functional theory[21−24] and an NBO population analysis[35−42] were used to predict the relative strengths and types of interactions occurring between the two molecules, and the results were correlated to experimental aggregation kinetics data at the 1:1 molar ratio of inhibitor: hIAPP (see the Details of the Calculations section). Computational costs prevented modeling other molar ratios.

Table 2 and Figure 4 compare the top three interactions for each hIAPP/inhibitor complex as well as the relative strength of each association. Each inhibitor was found to have several sites of interaction with hIAPP. The specific interactions seen, however, varied markedly between hIAPP and each inhibitor, as did the optimized conformation assumed by each peptide when binding hIAPP (see Supporting Information Figure S3 online). However, for those inhibitors possessing a glutamate residue, strong salt-bridge like interactions were seen with the Arg11 side chain of hIAPP. Additionally, only inhibitors-2 and -3 show interactions that span from the Arg11 side chain past the Phe15 side chain of hIAPP. All other compounds are primarily confined to a single section of the hIAPP molecule. We propose that this is one of the main reasons for the differences in

dx.doi.org/10.1021/ci300119c | J. Chem. Inf. Model. 2012, 52, 1298−1307

Table 2. Comparison of the Interface between hIAPP and Each Inhibitor

inhibitor	interaction[a] (hIAPP:Inh)	strength[b] (kcal/mol)	type	distance (Å)
1	His18−Tyr (OH)	68.20	H-bond	1.63
	Leu16 CO−C-term	28.26	H-bond	1.80
	Leu16 αC−C-term	11.03	H-bond-like	2.10
2	**Arg11−Glu**	**146.16**	**salt bridge**	**1.59**
	Leu16 CO−Tyr (OH)	61.84	H-bond	1.62
	Val17 αC−Tyr (OH)	9.14	H-bond-like	2.16
3	**Arg11−Glu**	**145.97**	**salt bridge**	**1.60**
	His18−C-term	18.12	H-bond	1.94
	Leu16 CO−Tyr βC	6.67	H-bond-like	2.19
4	**Arg11−Glu**	**74.56**	**salt bridge**	**1.72**
	Ala13 βC−Glu CO	8.84	H-bond-like	2.12
	Phe15 βC−Leu CO	6.92	H-bond-like	2.14
5	**Arg11−Glu**	**54.70**	**salt bridge**	**1.90**
	Thr9 NH−His CO	25.10	H-bond	1.83
	Gln10−Glu CO	23.40	H-bond	1.80

[a]OH = hydroxyl; CO = backbone carbonyl; NH = backbone amide nitrogen; αC = α-carbon; βC = β-carbon. [b]Strength is equated to the stabilization energy from the NBO perturbation analysis.

observed inhibitory capabilities. Inhibitor-4 does show interactions up to the Phe15 residue of hIAPP, but no interaction is seen that crosses this side chain. It seems therefore that spanning across this region of hIAPP may be the deciding factor in determining inhibitory capabilities at the 1:1 molar ratio.

From these results, it was observed that, at the 1:1 molar ratio, the strength of the salt bridge formed correlated directly with the ability of each inhibitor to slow aggregation. Figure 5 plots this relationship (R^2 = 0.966), showing that inhibitory efficacy at the 1:1 molar ratio is rationalized solely by the strength of the salt bridge formed. However, it was also noticed that inhibitors-2 and -3 (the only effective inhibitors at this molar ratio) were the only compounds to span hIAPP from the Arg11 side chain to past the Phe15 residue. We propose that this fact is also important in determining the effectiveness of our peptide inhibitors. An explanation that attempts to incorporate both factors is offered in the Discussion section.

Finally, because both slower aggregation and increased membrane damage were observed to be dependent on the concentration of inhibitor, we plotted the extent of membrane damage as a function of the change in aggregation kinetics (Figure 6). For most inhibitors (and for insulin), a surprisingly good linear fit was obtained, and overall, slower rates of hIAPP aggregation were associated with greater membrane damage. The significance of this is discussed below.

DISCUSSION

Attempts at inhibiting hIAPP aggregation with peptide-based inhibitors have had variable success,[43−45] despite the use of very different techniques and approaches to the problem. Scrocchi et al.[43] used short hexapeptides from the 20−29 region of hIAPP itself to inhibit aggregation. Like the peptides described in this study, they found that at sufficiently high concentrations (10× and 20× molar excess of inhibitor over hIAPP), inhibition could be achieved by most of the compounds they surveyed. However, inhibition at the 1:1 ratio occurred for only two of the molecules they used. Similarly, our lab was also only able to achieve inhibition at the 1:1 molar ratio with two peptides (inhibitors-2 and -3 here). Additionally, Scrocchi et al. found that some "inhibitors" substantially increased the rate of aggregation, comparable to the increased rate of fibrillogenesis seen here with inhibitors-1 and -5. In contrast, Yan et al.[45] used a full-length N-methylated derivative of hIAPP and reported complete inhibition of aggregation at nanomolar concentrations.

Taken together, these results suggest that we possess only a minimal understanding of the underlying forces behind protein aggregation and the processes occurring at the atomic level between hIAPP monomers that give rise to amyloid fibrils. The basis for the cytotoxicity of amyloid fibrils is also poorly understood. Membrane damage has been proposed as one of the main ways in which aggregates might destroy cells.[15−18] Consistent with other research,[1,2,5] our data using model liposome systems shows that slowing hIAPP aggregation is directly correlated with greater membrane damage (see Figure 6). This supports the conclusion that the aggregation process itself, rather than the mature fibrils, is the causative agent of membrane damage and therefore also a likely cause for cytotoxicity in vivo. Slowing this process may lead to prolonged cytotoxic exposure, ultimately causing greater membrane destruction. Alternatively, there may be more than one factor responsible for hIAPP-induced membrane damage.

Further, we have shown that the extent of membrane damage, as measured by dye leakage, is proportional to the concentration of inhibitor used and can be directly correlated with the change in the rate of aggregation brought about by the inhibitors. It is likely that, by slowing aggregation, these peptides increase the "lifetime" of a specific hIAPP species that damages the membrane. The inhibitors in this case may therefore function to create a scenario in which increased membrane damage can occur. This could come about by shifting the conformational equilibrium of hIAPP such that a particularly damaging conformer persists longer and is thus able to bring about more membrane damage.

The peptides assessed here represent increasingly longer stretches of the 10−18 region of the insulin B-chain (sequence HLVEALYLV), in which the core ALYLV sequence has been extended, one residue at a time from the N-terminus, in an attempt to find the smallest fragment with inhibitory properties and determine whether the negatively charged glutamate residue is important. Shorter sequences are both economically and synthetically advantageous and may serve as a framework for the rational design of small peptidomimetic inhibitors to the cytotoxicity of hIAPP. The fact that at sufficiently high molar ratios all compounds were able to slow aggregation to some extent (see Figure 3) suggests that we are utilizing the correct binding sequence and that each inhibitor is likely mimicking at least some of the same effects as the corresponding region of the full length B-chain of insulin. The results also imply that the series of peptides synthesized here act to slow hIAPP aggregation through the same mechanism as insulin; only the relative effectiveness of each compound differs.

However, a full understanding of the data requires an explanation for why the inhibitors have different effects at the same concentration. At the 1:1 molar ratio, only inhibitors-2 and -3 were effective (EALYLV and VEALYLV, respectively), and inhibitor-1 accelerated aggregation substantially (ALYLV).

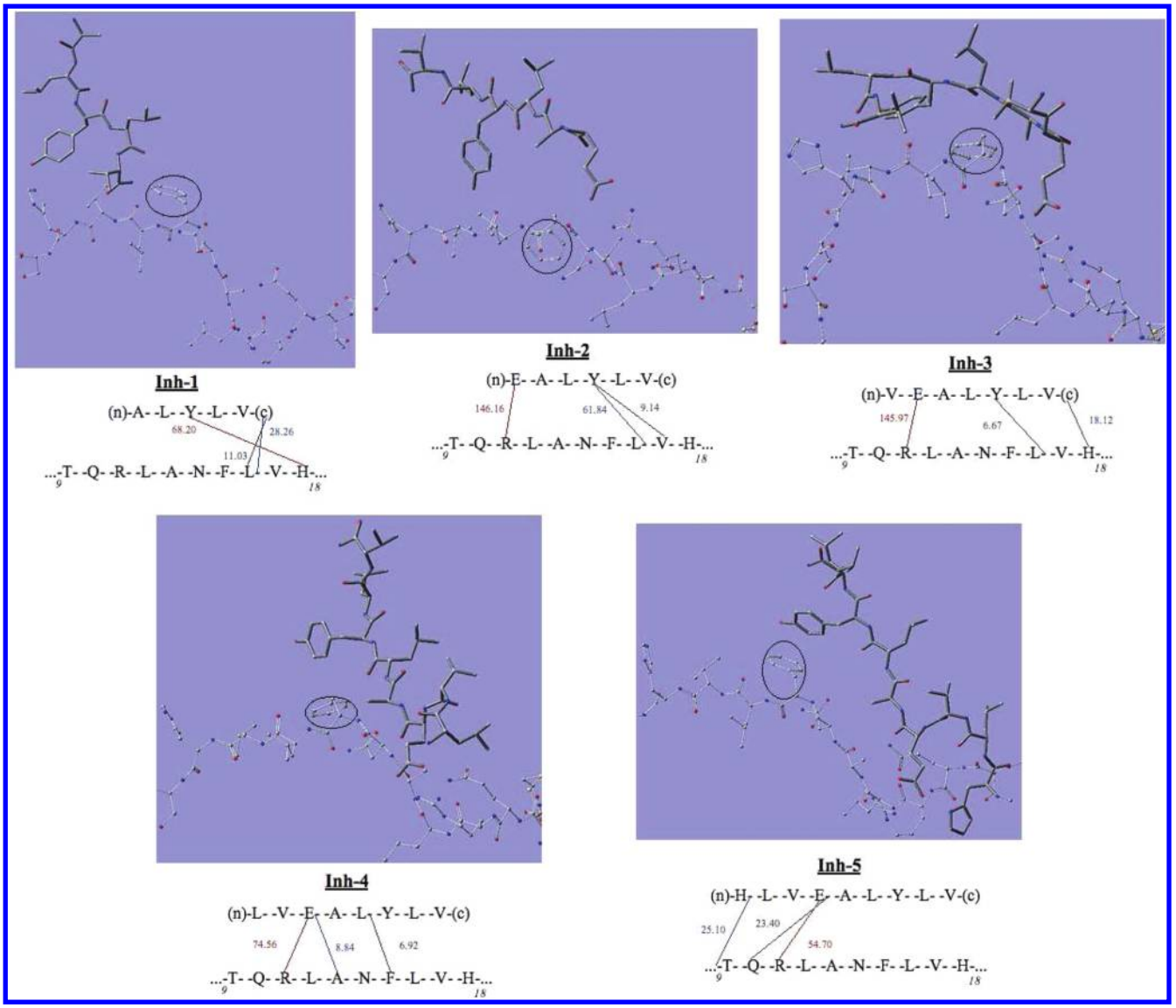

Figure 4. Results from geometry optimizations of each inhibitor/hIAPP complex, at the B3LYP/3-21G* level of theory. In all cases, hIAPP is oriented such that C-terminal residues are to the right, and the image is rotated to place the inhibitor (tube representation) "on top" of hIAPP (ball and stick model). Hydrogens are omitted for clarity, and only the interface region (residues 9−18 of hIAPP) is shown. Below each image is a schematic representation of the complex, showing the top three interactions. Letters indicate α-carbons or amino acid side chains. Dashes to the left of a letter represent the NH group of a peptide bond, while dashes to the right depict carbonyls. The labels (n) and (c) are amine and carboxamide termini, respectively, of the inhibitor. Only the portion of hIAPP involved in the interface is shown. Note that only inhibitors-2 and -3 show interactions spanning from the Arg11 side chain to beyond the Phe15 residue (dark circle) of hIAPP. We propose that this is one of the main reasons for the differences in observed inhibitory capabilities (See Figure 3; values are in kilocalories per mole; images constructed using GaussView[20]).

Wei et al.[14] have suggested that positively charged residues of IAPP near the N-terminus interact with Glu13 of the insulin B-chain. Wiltzius et al.[13] proposed that π-stacking between the Tyr16 (insulin) and Phe15 (hIAPP) side chains may be important for binding of the two molecules and that the Glu13 (insulin) and Arg11 (hIAPP) side chains are in proximity to one another.

The only difference between inhibitors-1 and -2 presented here is the addition of the negatively charged glutamate residue. At the 1:1 molar ratio, this difference apparently accounts for the full range of observed effects on aggregation kinetics (Figure 3). This suggests that in the simplest binding scenario (i.e., a 1:1 situation), the formation of the Arg−Glu salt bridge may be one of the principal determining factors in how strongly the molecules associate with one another. In computational studies, the only common interaction between hIAPP and each inhibitor was the formation of the Arg−Glu salt bridge (inhibitor-1 is the exception, as this compound does not possess a glutamate residue), and this interaction was the strongest measured for each hIAPP/inhibitor complex. Indeed, the ability to slow aggregation at the 1:1 molar ratio seems to be directly proportional to the strength of the Arg−Glu salt bridge that forms (Figure 5).

Interestingly, other research has found similar linear relationships in models studying DNA polymerases. Martinek et al.[46] found that the catalytic efficiency of DNA polymerase β correlated linearly with the hydrogen-bond strength between the Asn279 residue and the dCTP substrate, as calculated from molecular dynamics (MD). Zhang et al.[47] compared the efficiency of DNA polymerase with different purine analogs

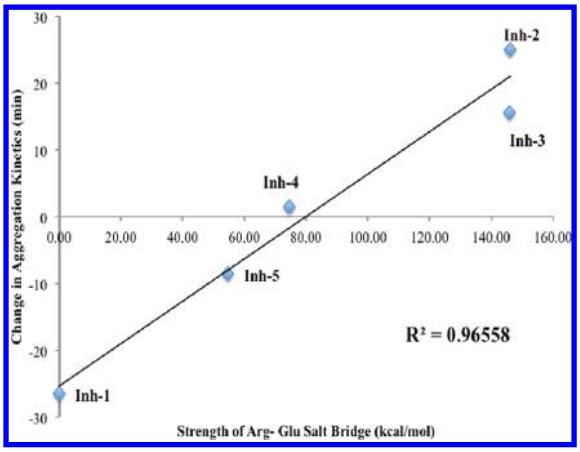

Figure 5. Change in rate of aggregation as a function of the strength of the Arg11−glutamate salt bridge (from Table 1). A good linear fit is obtained (R^2 = 0.966), suggesting that inhibitory capability is related to the strength of the Arg−Glu interaction formed between the inhibitors and hIAPP at 1:1 molar ratios.

substituted at C2 and, again, found a similar linear relationship. These findings may underscore an emerging pattern in select biomolecular complexes.

Although the strength of the salt bridge formed in our experiment explains the inhibitory trends observed at the 1:1 molar ratio very well, it was also noticed that inhibitors-2 and -3 formed associations with hIAPP along a greater stretch of the molecule compared to the other compounds. Specifically, these inhibitors spanned the region from the Arg11 side chain to past the Phe15 residue. Thus, not only were these peptides capable of "covering" a larger area of hIAPP, but they also covered a similar region. Because this area is one of the main amyloidogenic sections of hIAPP, it seems likely that the ability to bind strongly here is crucial to inhibiting aggregation for this series of peptides. Additionally, inhibitors-2 and -3 displayed several, separate interactions along this stretch of hIAPP, which should allow the molecules to remain bound longer and more strongly than the other compounds, as the transient loss of a single interaction can be offset by the other interactions keeping the molecule in place. In contrast, virtually all of the associations of both inhibitors-4 and -5 involved only the Arg11 side chain, and inhibitor-1 was confined primarily to the region of the His18 residue (Figure 4).

In part, the ability to bind hIAPP along this amyloidogenic region is a function of length. Inhibitor-1 is too short to span this area and does not possess any functionality capable of binding strongly to the hIAPP molecule. However, longer peptides such as inhibitors-4 and -5 are capable of greater conformational freedom; they can form numerous intramolecular associations and can become confined or "bunched up" at one region of hIAPP. Certainly, compounds-4 and -5 are *geometrically* capable of spanning this region of hIAPP; however, they may not be inclined to do so for thermodynamic reasons. At higher concentrations, however, these inhibitors were able to slow aggregation somewhat, and this may be due to the fact that if there are enough inhibitor molecules present in solution, at least some will adopt the proper conformation to bind along this stretch of hIAPP.

Covering this region likely prevents key interactions between hIAPP monomers that are necessary for aggregation. We suggest that the Phe15 side chain may play a critical role.

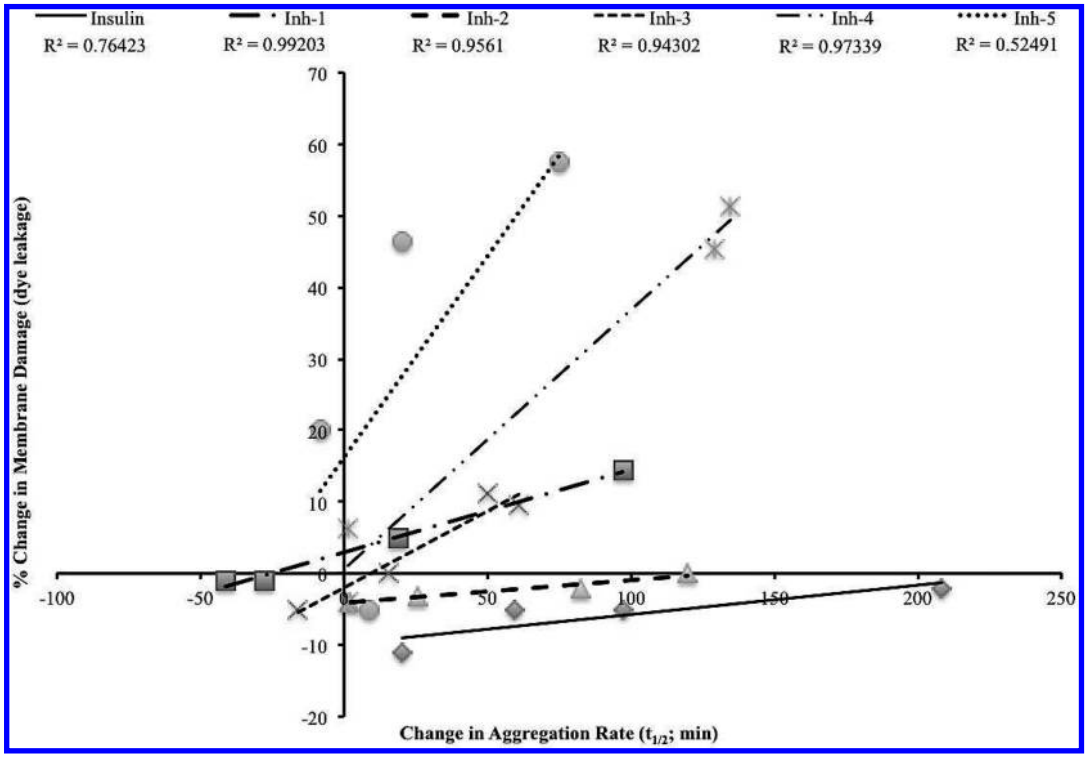

Figure 6. Change in membrane damage plotted as a function of the change in aggregation kinetics for each inhibitor (and insulin). Overall, membrane damage appears to correlate linearly with the extent to which each compound slows the rate of hIAPP aggregation, consistent with a model in which the aggregation process itself is responsible for cytotoxicity (as opposed to the mature aggregates). Only inhibitor-5 shows a poor fit, but the gross trend remains apparent.

Aromatic interactions have already been proposed to be important in amyloid formation,[48,49] though whether they function by contributing to self-assembly or by altering the kinetics of fibril formation is still being investigated. By changing the geometry of hIAPP around the Phe15 side chain, the inhibitors may act to prevent the proper alignment of aromatic residues of hIAPP molecules that are needed for aggregates to form or to elongate. It is also important to note that the 12−16 region of hIAPP has been shown to have the highest propensity to aggregate into β-sheet structures,[50] so it is reasonable that the inhibitors we find covering this region of hIAPP are also those that are better at slowing aggregation at 1:1 molar ratios.

In vitro, inhibitor-2 slowed aggregation to a greater extent than inhibitor-3 at all molar ratios. An explanation for this is desirable. Figure 7 below shows the electron density maps of the geometry-optimized structures of hIAPP with inhibitors-2 and -3. In the inhibitor-3/hIAPP complex, the hIAPP backbone shows a striking, ∼90° bend, which can be attributed to the interaction between the carboxamide-terminus of the inhibitor and the His18 side chain of hIAPP. In contrast, the inhibitor-2/hIAPP complex shows no such bend (no other inhibitor/hIAPP complex displayed this bend either, see Supporting Information Figure S3). One possible explanation for the observed difference in inhibitory capability between inhibitors-2 and -3 is that the geometry of the Phe15 side chain differs for each of these two complexes such that for inhibitor-3 the side chain is still somewhat "available" for aggregation. Another scenario, however, is that the strain induced by the sharp bend of the inhibitor-3/hIAPP complex is unfavorable enough that it lowers the ability of this compound to remain bound to hIAPP relative to inhibitor-2. This may also explain why inhibitor-3 does not reach the same level of inhibitory capability at higher molar ratios that the other compounds do. The formation of the bend is thermodynamically disfavored, enough that it works in opposition to binding hIAPP, thus preventing the compound from slowing aggregation to the same extent as the other inhibitors at higher molar ratios.

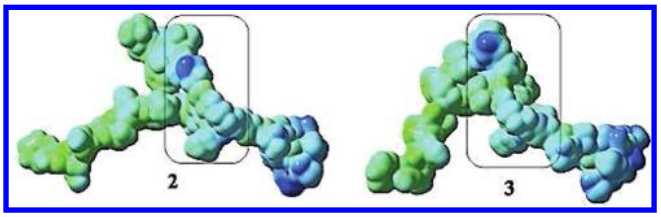

Figure 7. Electron density maps of the inhibitor-2 and inhibitor-3/hIAPP complexes, obtained by mapping the electrostatic potential onto the electron density of the optimized structure for each complex. Molecules were aligned as described in the Details of the Calculations section. The N-terminus of hIAPP is to the far right (positively charged, darker region), and the images are rotated to place inhibitors on top of hIAPP, tilted toward the viewer (gray box). Note that in the case of inhibitor-3, a sharp ∼90° bend is visible in the hIAPP backbone. No such bend is seen in the inhibitor-2/hIAPP complex. We propose that the steric strain brought about by bending hIAPP in this way may explain why inhibitor-3 was observed to have less inhibitory capability at all concentrations compared to inhibitor-2.

Conformational factors are obviously important in determining whether or not IAPP forms fibrils. Rat IAPP does not aggregate and is proline-rich along the 20−29 region, which restricts the conformations it can assume along this stretch of the molecule. It should also be noted that rat IAPP possesses a positively charged Arg18 residue in place of the His18 residue present in humans. This difference may serve to form an additional salt bridge with the Glu21 residue of the insulin B-chain and strengthen the binding between the molecules. Additionally, Hebda et al.[51] have combined the ideas of restricted conformational freedom and the formation of multiple salt bridges along the length of hIAPP to produce compounds that effectively inhibit its aggregation. Salt bridges were formed along the length of hIAPP from the N-terminus to the His18 side chain (four positively charged regions exist along this stretch of hIAPP). Thus, both salt bridge formation between molecules and the conformational freedom of hIAPP monomers (or between hIAPP and insulin) are likely crucial factors in the molecular interactions that influence IAPP aggregation.

It is worth noting here that we have drawn our conclusions based solely on density function methods. Another common approach to examining the behavior of large biomolecular systems is to use molecular dynamics (MD) simulations, which sample multiple minima along the potential energy surface.[52,53] While the results of DFT calculations are somewhat dependent on the choice of initial coordinates, they include the full range of quantum chemical effects that are absent from classical MD simulations. Comparisons of DFT and MD methods have been previously documented for a variety of chemical and biological systems, ranging from binding energies of cyclic decapeptides in inclusion complexes,[54] the effects of chain length on different spherical polymer brushes,[55] and bond distances in water and acetonitrile uranyl complexes.[56] In all cases, the results of MD and DFT calculations were found to be in good agreement, indicating that DFT can often serve as a valid alternative to MD simulations for large, biologically relevant systems.

Taken together, the experimental and computational data presented here suggest that two factors determine the effectiveness of our insulin-based inhibitors of hIAPP aggregation. The first is the ability to bind strongly to the Arg11 side chain, and the second is whether or not the compound contains some other group capable of binding "downstream", near the Phe15 residue. The apparent importance of the salt bridge, however, should not be underestimated. The only difference between inhibitors-1 and -2 is the presence of the glutamic acid residue—and this difference is able to account for the entire range of inhibitory capabilities demonstrated by the compounds investigated here. At the same time, however, it is clear that solely binding around the Arg11 side chain is insufficient to slow aggregation, since all inhibitors with a glutamate residue formed a salt bridge with the Arg11 side chain, yet had diverse effects on aggregation at the 1:1 molar ratio. It seems that the formation of the salt bridge is necessary only insofar as it permits positioning of the compound over hIAPP in such a way as to block amyloidogenic regions.

Finally, though the explanations offered here fit the data and explain the trends observed for the ability of each compound to slow amyloid formation, they do not explain why some inhibitors actually accelerate the aggregation process. This suggests that at least one other factor is in play in the association between hIAPP and the inhibitors. However, the answer to what this may be is not apparent from the current data. The geometry optimization calculations used here were carried out in the gas phase, and thus the molecules are modeled in a medium of low dielectric constant. When placed

into aqueous solution, however, the importance of the salt bridge will drop (as the dielectric constant rises) and other forces will increase in importance (in particular, hydrophobic interactions). Under the gas-phase and 1:1 molar ratio conditions of these density functional calculations, it seems likely that steric repulsion would strongly outweigh any thermodynamic benefit of van der Waals forces or π-stacking, and thus, these types of interactions may be difficult to "see" without modifying the parameters by which the molecules are investigated in silico.

It is also noteworthy that long-term incubation in vitro has shown that insulin can actually promote hIAPP aggregation by copolymerization of insulin and hIAPP monomers and oligomers.[57] The different roles of insulin in amyloid aggregation inhibition in healthy individuals and in aggregation promotion in pathogenic individuals implies that hIAPP and insulin likely play complex and significant roles in the onset of type-2 diabetes.[57] Uncovering the associations that lead to accelerated aggregation will further our understanding of protein aggregation in general and assist in designing more potent inhibitors.

■ ASSOCIATED CONTENT

Supporting Information

Table of mass spectra weights for each purified inhibitor in Table S1. Graph showing that dye leakage is proportional to inhibitor (or insulin) concentration in Figure S1; graph showing change in aggregation rate is proportional to inhibitor (or insulin) concentration in Figure S2; electron density maps for all five inhibitor/hIAPP complexes in Figure S3. This material is available free of charge via the Internet at http://pubs.acs.org/.

■ AUTHOR INFORMATION

Corresponding Author

*E-mail: dheylcle@emich.edu. Phone: (734) 487-2057. Fax: (734) 487-1496.

Notes

The authors declare no competing financial interest.

■ ACKNOWLEDGMENTS

This work was supported by an award of Research Corporation (DLH), by Eastern Michigan University, and used the Extreme Science and Engineering Discovery Environment (XSEDE), which is supported by the National Science Foundation grant number OCI-1053575.

■ REFERENCES

(1) Jaikaran, E.; Clark, A. Islet amyloid and type 2 diabetes: from molecular misfolding to islet pathophysiology. *Biochim. Biophys. Acta* **2001**, *1537*, 179−203.

(2) Larson, J. L.; Miranker, A. D. The mechanism of insulin action on islet amyloid polypeptide fiber formation. *J. Mol. Biol.* **2004**, *335*, 221−231.

(3) Padrick, S. B.; Miranker, A. D. Islet amyloid: phase partitioning and secondary nucleation are central to the mechanism of fibrillogenesis. *Biochemistry.* **2002**, *41*, 4694−4703.

(4) Hutton, J. C. The insulin secretory granule. *Diabetologia.* **1989**, *32*, 271−281.

(5) Gilead, S.; Wolfenson, H.; Gazit, E. Molecular mapping of the recognition interface between the islet amyloid polypeptide and insulin. *Angew. Chem., Int. Ed.* **2006**, *45*, 6476−6480.

(6) Glenner, G. G.; Eanes, E. D.; Wiley, C. A. Amyloid fibrils formed from a segment of the pancreatic-islet amyloid protein. *Biochem. Biophys. Res. Commun.* **1988**, *155*, 608−614.

(7) Westermark, P.; Engstrom, U.; Johnson, K. H.; Westermark, G. T.; Betsholtz, C. Islet amyloid polypeptide: pinpointing amino acid residues linked to amyloid fibril formation. *Proc. Natl. Acad. Sci. U.S.A.* **1990**, *87*, 5036−5040.

(8) Nilsson, M.; Raleigh, D. Analysis of amylin cleavage products provides new insights into the amyloidogenic region of human amylin. *J. Mol. Biol.* **1999**, *294*, 1375−1395.

(9) Jaikaran, E.; Higham, C. E.; Serpell, L. C.; Zurdo, J.; Gros, M.; Clark, A.; Fraser, P. E. Identification of a novel human islet amyloid polypeptide β-sheet domain and factors influencing fibrillogenesis. *J. Mol. Biol.* **2001**, *308*, 515−525.

(10) Gilead, S.; Gazit, E. The role of the 14−20 domain of the islet amyloid polypeptide in amyloid formation. *Exp. Diabetes Res.* **2008**, No. 256954, DOI: 10.1155/2008/256954.

(11) Kayed, R.; Bernhagen, J.; Greenfield, N.; Sweimeh, K.; Brunner, H.; Voelter, W.; Kapurniotu, A. Conformational transitions of islet amyloid polypeptide (IAPP) in amyloid formation in vitro. *J. Mol. Biol.* **1999**, *287*, 781−796.

(12) Jiang, P.; Wei, L.; Pervushin, K.; Mu, Y. pH-Dependent interactions of human islet amyloid polypeptide segments with insulin studied by replica exchange molecular dynamics simulations. *J. Phys. Chem.* **2010**, *114*, 10176−10183.

(13) Wiltzius, J.; Sievers, S.; Sawaya, M.; Eisenberg, D. Atomic structures of IAPP (amylin) fusions suggest a mechanism for fibrillation and the role of insulin in the process. *Protein Sci.* **2009**, *18*, 1521−1530.

(14) Wei, L.; Jiang, P.; Yau, Y. H.; Summer, H.; Shochat, S. G.; Mu, Y.; Pervushin, K. Residual structure in islet amyloid polypeptide mediates its interactions with soluble insulin. *Biochemistry* **2009**, *48*, 2368−2376.

(15) Brender, J. R.; Lee, E. L.; Cavitt, M. A.; Gafni, A.; Steel, D. G.; Ramamoorthy, A. Amyloid fiber formation and membrane disruption are separate processes localized in two distinct regions of IAPP, the type-2-diabetes-related peptide. *J. Am. Chem. Soc.* **2008**, *130*, 6424−6429.

(16) Khemtémourian, L.; Killian, J. A.; Höppener, J. W. M.; Engel, M. F. M. Recent insights in islet amyloid polypeptide-induced membrane disruption and its role in β-cell death in Type 2 Diabetes Mellitus. *Exp. Diabetes Res.* **2008**, No. 421287, DOI: 10.1155/2008/421287.

(17) Smith, P. E. S.; Brender, J. R.; Ramamoorthy, A. Induction of negative curvature as a mechanism of cell toxicity by amyloidogenic peptides: the case of islet amyloid polypeptide. *J. Am. Chem. Soc.* **2008**, *131*, 4470−4478.

(18) Heyl, D. L.; Osbourne, J. M.; Pamarthy, S.; Samisetti, S.; Gray, A. W.; Jayaprakash, A.; Konda, S. R.; Brown, D. J.; Miller, S. R.; Eizadkhah, R.; Milletti, M. C. Liposome damage and modeling of fragments of human islet amyloid polypeptide (IAPP) support a two-step model of membrane destruction. *Int. J. Peptide Res. Ther.* **2010**, *16*, 43−54.

(19) Frisch, M. J.; Trucks, G. W.; Schlegel, H. B.; Scuseria, G. E.; Robb, M. A.; Cheeseman, J. R.; Scalmani, G.; Barone, V.; Mennucci, B.; Petersson, G. A.; Nakatsuji, H.; Caricato, M.; Li, X.; Hratchian, H. P.; Izmaylov, A. F.; Bloino, J.; Zheng, G.; Sonnenberg, J. L.; Hada, M.; Ehara, M.; Toyota, K.; Fukuda, R.; Hasegawa, J.; Ishida, M.; Nakajima, T.; Honda, Y.; Kitao, O.; Nakai, H.; Vreven, T.; Montgomery, Jr., J. A.; Peralta, J. E.; Ogliaro, F.; Bearpark, M.; Heyd, J. J.; Brothers, E.; Kudin, K. N.; Staroverov, V. N.; Kobayashi, R.; Normand, J.; Raghavachari, K.; Rendell, A.; Burant, J. C.; Iyengar, S. S.; Tomasi, J.; Cossi, M.; Rega, N.; Millam, N. J.; Klene, M.; Knox, J. E.; Cross, J. B.; Bakken, V.; Adamo, C.; Jaramillo, J.; Gomperts, R.; Stratmann, R. E.; Yazyev, O.; Austin, A. J.; Cammi, R.; Pomelli, C.; Ochterski, J. W.; Martin, R. L.; Morokuma, K.; Zakrzewski, V. G.; Voth, G. A.; Salvador, P.; Dannenberg, J. J.; Dapprich, S.; Daniels, A. D.; Farkas, Ö.; Foresman, J. B.; Ortiz, J. V.; Cioslowski, J.; Fox, D. J. *Gaussian 09*, Revision C.02; Gaussian, Inc., Wallingford CT, 2009.

(20) *GaussView*, version 2.1; Gaussian, Inc.: Wallingford, CT, 2000.

(21) Hohenberg, P.; Kohn, W. Inhomogeneous Electron Gas. *Phys. Rev.* **1964**, *136*, B864−B871.
(22) Kohn, W.; Sham, L. J. Self-Consistent Equations Including Exchange and Correlation Effects. *Phys. Rev.* **1965**, *140*, A1133−A1138.
(23) Parr, R. G.; Yang, W. *Density-functional theory of atoms and molecules*; Oxford Univ. Press: Oxford, 1989.
(24) *The Challenge of d and f Electrons*; Salahub, D. R., Zerner, M. C., Eds.; American Chemical Society: Washington, D.C., 1989.
(25) Becke, A. D. Density-functional thermochemistry. III. The role of exact exchange. *J. Chem. Phys.* **1993**, *98*, 5648−5652.
(26) Lee, C.; Yang, W.; Parr, R. G. Development of the Colle-Salvetti correlation-energy formula into a functional of the electron density. *Phys. Rev. B.* **1988**, *37*, 785−789.
(27) Miehlich, B.; Savin, A.; Stoll, H.; Preuss, H. Results obtained with the correlation-energy density functionals of Becke and Lee, Yang and Parr. *Chem. Phys. Lett.* **1989**, *157*, 200−206.
(28) Vosko, S. H.; Wilk, L.; Nusair, M. Accurate spin-dependent electron liquid correlation energies for local spin density calculations: A critical analysis. *Can. J. Phys.* **1980**, *58*, 1200−1211.
(29) Binkley, J. S.; Pople, J. A.; Hehre, W. J. Self-Consistent Molecular Orbital Methods. 21. Small Split-Valence Basis Sets for First-Row Elements. *J. Am. Chem. Soc.* **1980**, *102*, 939−947.
(30) Gordon, M. S.; Binkley, J. S.; Pople, J. A.; Pietro, W. J.; Hehre, W. J. Self-Consistent Molecular Orbital Methods. 22. Small Split-Valence Basis Sets for Second-Row Elements. *J. Am. Chem. Soc.* **1982**, *104*, 2797−2803.
(31) Pietro, W. J.; Francl, M. M.; Hehre, W. J.; Defrees, D. J.; Pople, J. A.; Binkley, J. S. Self-Consistent Molecular Orbital Methods. 24. Supplemented small split-valence basis-sets for 2nd-row elements. *J. Am. Chem. Soc.* **1982**, *104*, 5039−5048.
(32) Dobbs, K. D.; Hehre, W. J. Molecular-orbital theory of the properties of inorganic and organometallic compounds. 4. Extended basis-sets for 3rd row and 4th row, main-group elements. *J. Comput. Chem.* **1986**, *7*, 359−378.
(33) Dobbs, K. D.; Hehre, W. J. Molecular-orbital theory of the properties of inorganic and organometallic compounds. 5. Extended basis-sets for 1st-row transition-metals. *J. Comput. Chem.* **1987**, *8*, 861−879.
(34) Dobbs, K. D.; Hehre, W. J. Molecular-orbital theory of the properties of inorganic and organometallic compounds. 6. Extended basis-sets for 2nd-row transition-metals. *J. Comput. Chem.* **1987**, *8*, 880−893.
(35) Foster, J. P.; Weinhold, F. Natural hybrid orbitals. *J. Am. Chem. Soc.* **1980**, *102*, 7211−7218.
(36) Reed, A. E.; Weinhold, F. Natural bond orbital analysis of near-Hartree-Fock water dimer. *J. Chem. Phys.* **1983**, *78*, 4066−4073.
(37) Reed, A. E.; Weinstock, R. B.; Weinhold, F. Natural-population analysis. *J. Chem. Phys.* **1985**, *83*, 735−746.
(38) Reed, A. E.; Weinhold, F. Natural Localized Molecular Orbitals. *J. Chem. Phys.* **1985**, *83*, 1736−1740.
(39) Carpenter, J. E. *Extension of Lewis structure concepts to open-shell and excited-state molecular species*. Ph. D. thesis, University of Wisconsin, Madison, WI, 1987.
(40) Carpenter, J. E.; Weinhold, F. Analysis of the geometry of the hydroxymethyl radical by the different hybrids for different spins natural bond orbital procedure. *J. Mol. Struct. (Theochem)* **1988**, *46*, 41−62.
(41) Reed, A. E.; Curtiss, L. A.; Weinhold, F. Intermolecular interactions from a natural bond orbital, donor-acceptor viewpoint. *Chem. Rev.* **1988**, *88*, 899−926.
(42) Weinhold, F.; Carpenter, J. E. In *The Structure of Small Molecules and Ions*; Naaman, R., Vager, Z., Eds.; Plenum: New York, 1988; pp 227−236.
(43) Scrocchi, L. A.; Chen, Y.; Waschuk, S.; Wang, F.; Cheung, S.; Darabie, A. A.; McLaurin, J.; Fraser, P. E. Design of peptide-based inhibitors of human islet amyloid polypeptide fibrillogenesis. *J. Mol. Biol.* **2002**, *318*, 697−706.
(44) Scrocchi, L. A.; Chen, Y.; Wang, F.; Han, K.; Ha, K.; Wu, L.; Fraser, P. E. Inhibitors of islet amyloid polypeptide fibrillogenesis, and the treatment of typ-2 diabetes. *Lett. Peptide Sci.* **2003**, *10*, 545−551.
(45) Yan, L. M.; Tatarek-Nossol, M.; Velkova, A.; Kazantzis, A.; Kapurniotu, A. Design of a mimic of nonamyloidogenic and bioactive human islet amyloid polypeptide (IAPP) as nanomolar affinity inhibitor of IAPP cytotoxic fibrillogenesis. *Proc. Natl. Acad. Sci. U.S.A.* **2006**, *103*, 2046−2051.
(46) Martinek, V.; Bren, U.; Goodman, M. F.; Warshel, A.; Florian, J. DNA polymerase β catalytic efficiency mirrors the Asn279-dCTP H-bonding strength. *FEBS Lett.* **2007**, *581*, 775−780.
(47) Zhang, H.; Bren, U.; Kozekov, I. D.; Rizzo, C. J.; Stec, D. F.; Guengerich, F. P. Steric and electrostatic effects at the C2 atom substituent influence replication and miscoding of the DNA deamination product deoxyxanthosine and analogs by DNA polymerases. *J. Mol. Biol.* **2009**, *392*, 251−269.
(48) Gazit, E. A possible role for π-stacking in the self-assembly of amyloid fibrils. *FASEB J.* **2002**, *16*, 77−83.
(49) Milardi, D.; Sciacca, M.; Pappalardo, M.; Grasso, D. M.; La Rosa, C. The role of aromatic side-chains in amyloid growth and membrane interaction of the islet amyloid polypeptide fragments LANFLVH. *Eur. Biophys. J.* **2011**, *40*, 1−12.
(50) Cecchini, M.; Curcio, R.; Pappalardo, M.; Melki, R.; Caflisch, A. A molecular dynamics approach to the structural characterization of amyloid aggregation. *J. Mol. Biol.* **2006**, *357*, 1306−1321.
(51) Hebda, J. A.; Saraogi, I.; Magzoub, M.; Hamilton, A. D.; Miranker, A. D. A peptidomimetic approach to targeting pre-amyloidogenic states in Type II Diabetes. *Chem. Biol.* **2009**, *16*, 943−950.
(52) Udommaneethanakit, T.; Rungrotmongkol, T.; Bren, U.; Frecer, V.; Stanislav, M. Dynamic behavior of avian influenza A virus neuraminidase subtype H5N1 in complex with oseltamivir, zanamivir, peramivir, and their phosphonate analogues. *J. Chem. Info. Model.* **2009**, *49*, 2323−2332.
(53) Bren, U.; Lah, J.; Bren, M.; Martinek, V.; Florian, J. DNA duplex stability: the role of preorganized electrostatics. *J. Phys. Chem.* **2010**, *114*, 2876−2885.
(54) Zhao, H.; Zhu, Y.; Tong, M.; He, J.; Liu, C.; Tang, M. Density functional theory studies on the inclusion complexes of cyclic decapeptide with 1-phenyl-1-propanol enantiomers. *J. Mol. Model.* **2012**, *18*, 851−858.
(55) Lo Verso, F.; Egorov, S. A.; Milchev, A.; Binder, K. Spherical polymer brushes under good solvent conditions: molecular dynamics results compared to density functional theory. *J. Phys. Chem.* **2010**, 184901 DOI: 10.1063/1.3494902.
(56) Buhl, M.; Sieffert, N.; Chaumont, A.; Wipff, G. Water versus acetonitrile coordination to uranyl. Density functional study of cooperative polarization effects in solution. *Inorg. Chem.* **2011**, *50*, 299−308.
(57) Cui, W.; Ma, J. W.; Lei, P.; Wu, W. H.; Yu, Y. P.; Xiang, Y.; Tong, A. J.; Zhao, Y. F.; Li, Y. M. Insulin is a kinetic but not a thermodynamic inhibitor of amylin aggregation. *FEBS J.* **2009**, *276*, 3365−3371.